รหัสโครงการ SUT1-107-56-12-39

รายงานการวิจัย

การวิเคราะห์รูปทรงสามมิติแบบดิจิตอลฟูริเยร์ทรานฟอร์มโดยตัวกรองเวฟเล็ท

Digital Fourier Transform Profilometry Using Wavelet Filter

ได้รับทุนอุดหนุนการวิจัยจาก
มหาวิทยาลัยเทคโนโลยีสุรนารี

ผลงานวิจัยเป็นความรับผิดชอบของหัวหน้าโครงการวิจัยแต่เพียงผู้เดียว

รหัสโครงการ SUT1-107-56-12-39

รายงานการวิจัย

การวิเคราะห์รูปทรงสามมิติแบบดิจิตอลฟูริเยร์ทรานฟอร์มโดยตัวกรองเวฟเล็ท

Digital Fourier Transform Profilometry Using Wavelet Filter

ผู้วิจัย

หัวหน้าโครงการ

Prof. Dr. Joewono Widjaja

สาขาวิชาฟิสิกส์

สำนักวิชาวิทยาศาสตร์

ได้รับทุนอุดหนุนการวิจัยจากมหาวิทยาลัยเทคโนโลยีสุรนารี ปีงบประมาณ 2556-2557

ผลงานวิจัยเป็นความรับผิดชอบของหัวหน้าโครงการวิจัยแต่เพียงผู้เดียว

กรกฎาคม 2559

Acknowledgement

The principal investigator acknowledges the research grant supported by the Suranaree University of Technology.

บทคัดย่อ

งานวิจัยนี้ศึกษาการกำจัดพื้นหลังในฟูเรียร์ทรานฟอร์มโปรฟิโลเมทรีโดยใช้อนุพันธ์ลำดับที่หนึ่งและลำดับที่สองของเวฟเลทชนิดเกาส์เซียน ซึ่งข้อดีของการใช้เวฟเลทชนิดเกาส์เซียนเมื่อเทียบกับกระบวนการปกติคือ สามารถกำจัดสัญญาณพื้นหลังไปพร้อมๆกับการคัดเลือกความถี่มูลฐานที่ใช้ในการสกัดข้อมูลเฟส ผลการทดลองแสดงให้เห็นว่าการวัดความสูงสามมิติโดยใช้อนุพันธ์ลำดับที่สองของเกาส์เซียนเวฟเล็ทให้ผลที่แม่นยำกว่าการใช้อนุพันธ์ลำดับที่หนึ่ง

Abstract

Background elimination in Fourier transform profilometry by using first and second derivatives of Gaussian wavelets are studied. The advantage of the Gaussian wavelets over the conventional method is that it can simultaneously eliminate the background signal and select fundamental frequency used for phase extraction. Experimental results show that 3D height measurements by using the second derivative Gaussian wavelet is more accurate than the first derivative.

Contents

List of Figures

Chapter 1
Introduction

1.1 Background and Significance

Non contact and non invasive abilities of optical measurement techniques have found growing interest in three-dimensional (3D) shape measurement and imaging such as object modeling, medical diagnostics, computer-aided design and computer-aided manufacturing. One of these optical methods is Fourier transform profilometry (FTP) [1-6]. The FTP has found various applications in diverse fields such as biomedical applications [7-11], quality control of printed circuit board manufacturing [12-16], kinematic study of a moving creature [17-19], cultural heritage and preservation [20,21], global measurement of free surface deformations [22,23], and biometric identification [24] etc.

The FTP reconstructs the 3D object profile by projecting a Ronchi grating or a sinusoidal grating pattern onto a specimen being studied. A grating pattern deformed by height variations is captured by an image sensor camera. As a result, height variations of the object surface modulate phase information of the grating pattern. Therefore, the key to this shape measurement technique is accuracy and reliability of the phase extraction. In order to extract the phase modulation, Fourier transform of a 1D signal of the deformed grating captured by the CCD is computed. After filtering only the fundamental spatial-frequency spectrum component via a rectangular band-pass filter and subsequently taking its inverse Fourier transform, the height information can be decoded from the extracted phase [1,2]. The conventional FTP has a drawback in that firstly, high slope object will cause deep phase modulation, broadening the desired fundamental spatial-frequency spectrum. As the result, the fundamental and the zero-order spectra overlap. This limits measurable heights. Secondly, the rectangular filter which has sharp frequency responses will degrade fine details of the reconstructed 3D surface profile. This is because the filter has an oscillatory impulse response of sinc function in the space domain which is known as the ringing artifacts.

Recently, methods for solving this drawback by using a wavelet transform (WT) [25,26] have been reported. On the basis of its multi-resolution property, the WT analyzes an input signal by using a bank of wavelet filters generated from a unique function which has a response of band-pass filter. By taking an advantage of this band-pass nature, the unwanted zero-order spectrum can be eliminated, while the desired fundamental spectrum can be simultaneously filtered to give the phase information. Therefore, dynamic 3D profiles can be reconstructed by using a single computation of the wavelet analysis. This is evidently faster than the conventional FTP. A main

concern of the frequency domain processing is that precise extraction of the fundamental frequency is hardly achieved when bandwidth of the deformed grating image is broad. In this project, the 3D shape reconstruction from the deformed grating images by using wavelet transform (WT) is studied by employing first- and second-order derivatives of Gaussian functions which have different frequency responses. Measurement performance of the proposed methods will be compared with that of the conventional technique.

1.2 Objectives

1. To verify feasibility of 3D height reconstruction by using the WT method
2. To develop software for extracting phase modulation and reconstructing 3D height
3. To compare the proposed and the conventional methods

1.3 Scope

In this study, a sinusoidal grating digitally generated by using a LCD projector is projected onto a 3D test object. Firstly, grating patterns deformed by the object and the reference plane are captured by a CCD camera connected to a computer system. Secondly, the two grating images deformed by the object and the reference plane are wavelet transformed by using the first- and the second-order derivatives of the Gaussian function at an appropriate dilation factor. This step removes simultaneously the background information and the ringing artifacts. Desired phase modulation is then extracted from the background-eliminated deformed gratings. After unwrapping the phase, the height distribution is reconstructed. The determination of the phase modulation and the 3D reconstruction is done by using Matlab 6.0. Calibration of the system will be done by utilizing a 3D triangular prism with known dimension.

1.4 Expected Benefit

1.4.1 The result of this research project is useful for electronic manufacturers, automation industries, health care and medical diagnostics, cultural heritage and preservation, security etc.

1.4.2 Participation of graduate students as research assistant provides an opportunity for developing manpower with capability to conduct research in the area of science, medicine and engineering.

Chapter 2

3D Height Reconstruction Using Wavelet Filter

2.1 Fourier Transform Profilometry

Figure 1 shows a schematic diagram of crossed-optical-axes setup for implementing the grating-based profilometry. A LCD projector is used to project a sinusoidal grating pattern stored in a computer system. The grating images deformed by the object being measured and the reference plane are given by

$$g_1(x,y) = o(x,y) + bo(x,y)\cos[2\pi f_0 x + \phi(x,y)] \tag{1}$$

and

$$g_2(x,y) = r(x,y) + br(x,y)\cos[2\pi f_0 x + \phi_0(x,y)], \tag{2}$$

respectively. Here, $o(x,y)$ and $r(x,y)$ correspond to the irradiances caused by non-uniform light reflection of the object and the reference plane, respectively. In the above equations, f_0 stands for the carrier frequency of the observed grating image, while b is the modulation factor. $\phi(x,y)$ and $\phi_0(x,y)$ are the phase modulations arising from the height profile of the object and the reference plane, respectively. Note that the higher the profile, the broader the phase modulation.

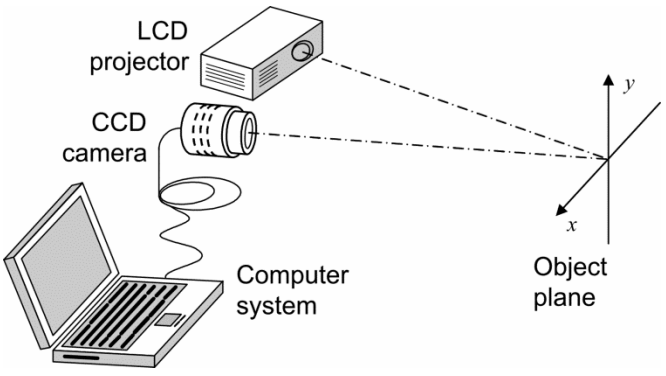

Figure 2.1 A schematic diagram of an optical setup for implementing the FTP-based profilometry by using the wavelet filters.

In the FTP, the phase modulation $\phi(x,y)$ is extracted in the spatial frequency domain by using Fourier transform. For the sake of simplicity, Eq. (1) can be mathematically rewritten as

$$g_1(x,y) = o(x,y) + c(x,y)\exp(+i2\pi f_0 x) + c^*(x,y)\exp(-i2\pi f_0 x) \tag{3}$$

where

$$c(x,y) = 0.5bo(x,y)\exp[\,i\phi(x,y)]\,. \tag{4}$$

A 1-D Fourier transformation of Eq. (3) with respect to the *x* direction can be mathematically expressed as

$$G_1(f_x,y) = O(f_x,y) + C(f_x - f_0,y) + C^*(f_x + f_0,y), \tag{5}$$

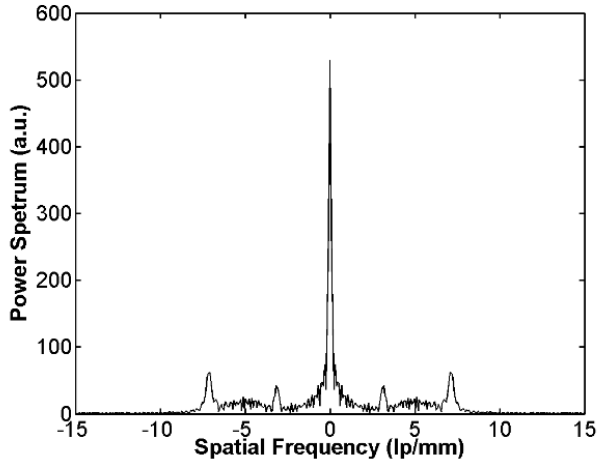

Figure 2.2 Power spectrum of a 1D signal scanned from a typical grating pattern deformed by 3D object.

where the first, the second and the third terms of Eq. (5) are the 1-D Fourier spectra of the non-uniform reflected light $o(x,y)$, $c(x,y)$ and $c^*(x,y)$, respectively. Figure 2.2 shows a typical power spectral distribution $G_1(f_x,y)$ of Eq. (5). The first term which appears at the origin is known as the zero-order spectrum, while the second and the third terms correspond to the $+1^{st}$ and the -1^{st} orders of the frequency spectra, respectively. They are separated from the zero-order spectra by the carrier frequency f_0. According to Eq. (5), the desired phase modulation $\phi(x,y)$ is encoded into the $+1^{st}$ and the -1^{st} fundamental frequency spectra. The 3-D shape can be accurately measured, provided the fundamental spectra are not corrupted by the zero-order spectrum. When there is no spectral overlapping, filtering one of the fundamental spectra such as $C(f_x - f_0,y_0)$ can be done by using the rectangular band-pass filter. An inverse Fourier transformation of the filtered spectrum gives a complex signal

$$g_1'(x,y) = 0.5bo(x,y)\exp\{i[2\pi f_0 x + \phi(x,y)]\}. \tag{6}$$

By applying the same filtering to the grating image deformed by the reference plane, a second complex signal

$$g_2'(x,y) = 0.5br(x,y)\exp\{i[2\pi f_0 x + \phi_0(x,y)]\} \tag{7}$$

is produced. The carrier frequency can be eliminated by taking a product of Eq. (6) and a complex conjugate of Eq. (7)

$$g_1'(x,y)\cdot g_2'^{*}(x,y) = 0.25b^2 o(x,y)r(x,y)\exp\{i[\phi(x,y)-\phi_0(x,y)]\}. \tag{8}$$

The phase modulation due to the object height distribution is extracted by calculating a complex logarithm of Eq. (8)

$$\log[g_1'(x,y)\cdot g_2'^{*}(x,y)] = \log[0.25b^2 o(x,y)r(x,y)] + i[\phi(x,y)-\phi_0(x,y)]. \tag{9}$$

The phase difference $\phi(x,y)-\phi_0(x,y)$ in the imaginary part is completely separated from the unwanted amplitude variation $b^2 o(x,y)r(x,y)$ in the real part. Finally, the height distribution is calculated according to

$$h(x,y) = \frac{l_0[\phi(x,y)-\phi_0(x,y)]}{[\phi(x,y)-\phi_0(x,y)]-2\pi f_0 d}, \tag{10}$$

where l_0 and d are the separation distances between the CCD camera and the reference plane and between the camera and the projector, respectively.

2.2 Wavelet Transform

The wavelet transform (WT) is a mathematical technique which has been introduced in signal analysis to overcome the inability of Fourier analysis in providing local frequency spectra. The definition of the WT of a spatial signal $g(x)$ is given by [27]

$$W_g(a,b) = \frac{1}{\sqrt{a}}\int_{-\infty}^{+\infty} g(x)h^{*}\left(\frac{x-b}{a}\right)dx, \tag{11}$$

where a and b are the dilation and the translation parameters, respectively. This equation can be interpreted as a cross correlation between the signal $g(x)$ and a set of elementary functions derived by dilating the mother wavelet $h(x)$ which has a response of band-pass filter. When the signal $g(x)$ has the same frequency content as that of the dilated analyzing wavelet $h(x/a)$ in the region subtended by $h^{*}[(x-b)/a]$, a correlation peak is generated in the WT domain. Thus, the WT of the signal $g(x)$ is a description of the signal across a range of frequencies. The resultant WT gives many wavelet coefficients which are a function of the dilation and the position. Since the WT is

computed at given continuous values of the dilation and the translation, this type of WT is called the continuous WT.

There are two Gaussian wavelets which are widely used for signal and image analysis [25,26]. The first wavelet is the first-order derivative of the Gaussian function given by

$$h(x) = \frac{-x}{\sigma^3\sqrt{2\pi}} \exp\left(-\frac{x^2}{2\sigma^2}\right). \tag{12}$$

The second one is the second-order derivative of the Gaussian function or the so-called Mexican hat wavelet defined as [27]

$$h(x) = \frac{1}{\sigma^3\sqrt{2\pi}}\left(\frac{x^2}{\sigma^2} - 1\right) \exp\left(-\frac{x^2}{2\sigma^2}\right). \tag{13}$$

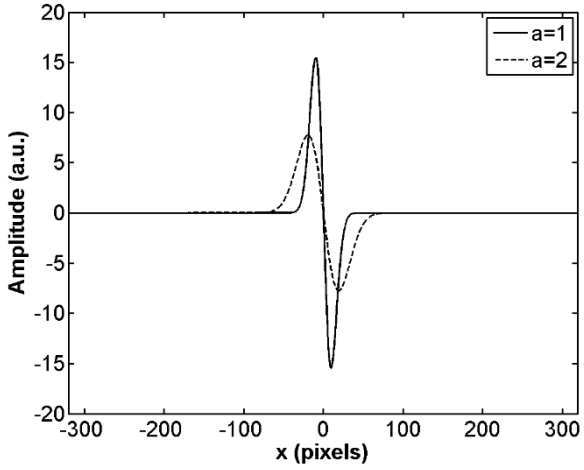

(a)

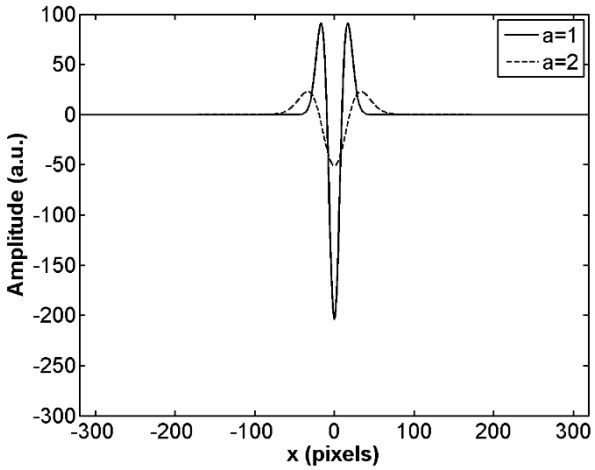

(b)

Figure 2.3 (a) First- and (b) second-order derivatives of the Gaussian functions, respectively.

Figures 2.3(a) and (b) illustrate the first-order derivative of the Gaussian function and the Mexican hat wavelet for different scale factors. Their spatial widths can be varied by changing the dilation factors. The small dilation compresses the wavelet signal, while the large one causes a wavelet dilation. The changes of the signal width in the space domain will affect its frequency responses. The mother wavelet $h(x)$ must satisfy the admissible condition such as

$$\left|H_a(af_x)\right|^2 = 0 \text{ for } f_x = 0 \tag{14}$$

and

$$\int_{-\infty}^{\infty} h(x)dx = 0. \tag{15}$$

These condition show that the mean of the mother wavelet must equal to zero or its spectrum $H(f_x)$ has a zero dc component.

In the spatial frequency domain, Eq. (11) can be rewritten as

$$W_g(a,b) = \sqrt{a}\int_{-\infty}^{+\infty} G(f_x)H_a^*(af_x)\exp(i2\pi bf_x)df_x\ , \tag{16}$$

which is calculated by taking an inverse Fourier transform of a product of two spectra of the signal $g(x)$ and the wavelet $h(x)$ dilated by the factor a. By varying the dilation of the analyzing wavelet, the signal $g(x)$ is analyzed via a set of band-pass filters having different center frequency and pass-band.

Figures 2.4(a) and (b) show the corresponding frequency responses of the two Gaussian wavelets for different dilation factors. It is obvious that besides these filters are concentrated in the space and the spatial frequency domains, their amplitudes vary smoothly. The admissible condition can be employed for eliminating the zero-order spectrum and simultaneously localize the desired fundamental frequency components of the deformed grating signals. Therefore, the ringing artifacts will not occur in the spatial domain of the reconstructed shape. Furthermore, the spectral plots also reveal that the small dilation factor produces a band-pass filter with high center frequency and broad pass-band. For a large dilation factor, the center frequency and the pass-band reduce. If the spatial width and the bandwidth of the wavelet function are regarded as the spatial and the frequency resolutions, respectively, the small dilation factor corresponds to the wavelet analysis with high spatial resolution and low frequency resolution. In contrast, the high dilation caused an analysis with low spatial resolution and high frequency resolution. This is known as the multi-resolution property of the WT. Due to this property, the unwanted zero-order spectrum of the deformed grating patterns can be eliminated, whereas, its desired fundamental spectrum can be localized for the phase extraction without causing the ringing artifact as the conventional FTP.

Further comparisons of the frequency responses of the two wavelet filters reveal that firstly they have different center frequencies and width of pass-bands. These are caused by the fact that

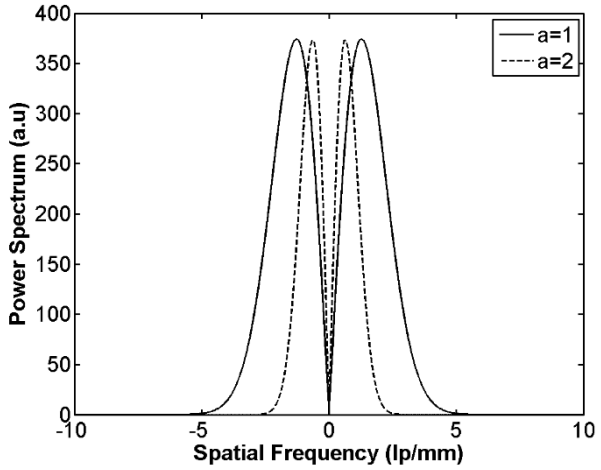

(a)

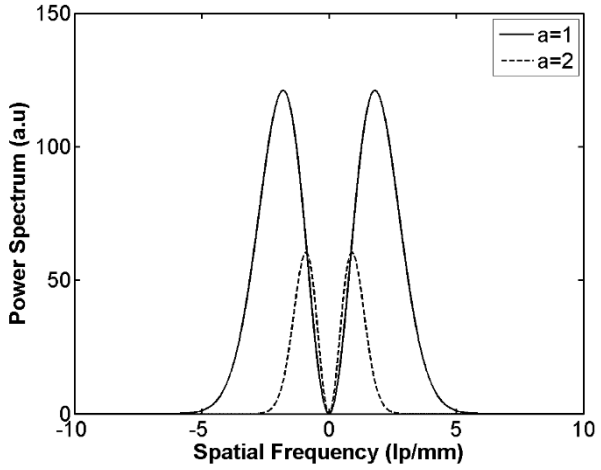

(b)

Figure 2.4 Frequency responses of (a) the first- and (b) the second-order derivatives of the Gaussian functions, respectively.

the frequency response around the low cutoff-frequency of the first-order derivative of the Gaussian wavelet varies linearly, instead of nonlinear variation of the Mexican hat wavelet. Secondly, the amplitude of the frequency spectrum of the first-order derivative of the Gaussian wavelet is higher and less affected by the changing of the dilation factor than that of the Mexican hat wavelet. Thus, the first-order derivative of the Gaussian function may not be effective for suppressing low frequency components of the deformed grating patterns. Since these differences

may affect the reconstructed 3-D profiles, the present work studies the reconstruction performance of the two wavelet filters.

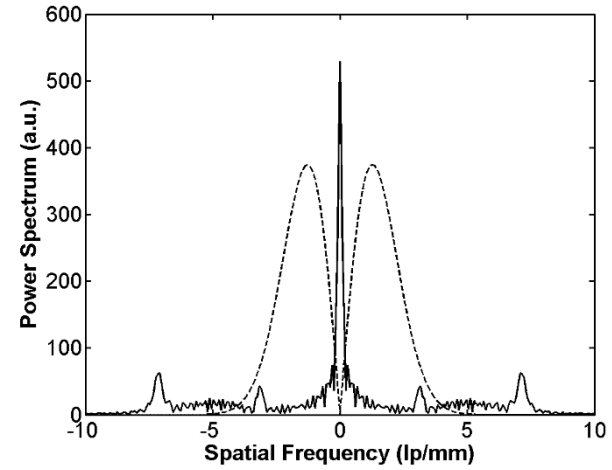

(a)

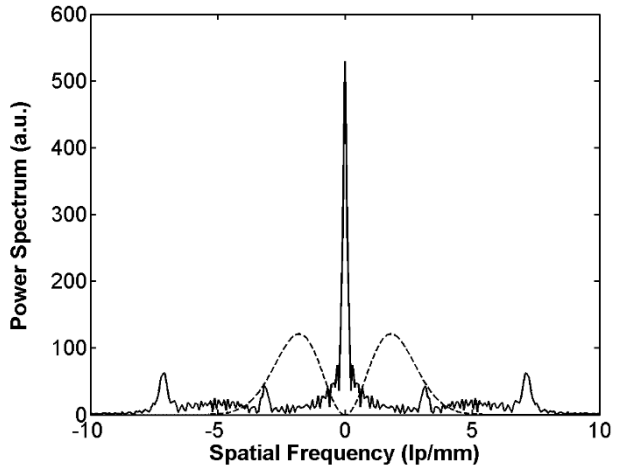

(b)

Figure 2.5 Frequency localization of the deformed grating pattern by using (a) the first- and (b) the second-order derivatives of the Gaussian functions, respectively.

Figures 2.5(a) and (b) illustrate the effects of applying the first-order derivative of the Gaussian and the Mexican hat wavelets to the frequency spectrum $G(f_x,y)$ of the deformed grating pattern. The dot lines represents the frequency responses of the wavelets. In this figure, an area of the spectrum of the deformed grating overlapped by that of the wavelet filter corresponds the spectral localization where the phase information will be extracted. The first effect is related to the low cutoff-frequency response of the two wavelets. When the first-order derivative of the Gaussian wavelet is employed, the low frequency components of the zero-order spectrum of the

deformed grating patterns is not completely eliminated, due to the linear frequency response around the zero frequency. This means that the unwanted background signal still exist. As consequences, the desired fundamental spectrum may be overlapped by the zero-order spectrum. The second effect can be observed from Fig. 2.5(b) which shows that when the Mexican hat wavelet is used for localization of the fundamental spectrum, more low frequency components of the deformed grating pattern are suppressed. Therefore, it is important to verify experimentally the reconstruction performance of the two wavelets.

Chapter 3
Materials and Methods

In order to conduct our study of the 3D profilometry by suing the wavelet filters, the FTP setup shown in Fig. 3.1 was constructed by using a LCD projector (Toshiba TLP-X2000) with resolution 1024 × 768 pixels and a CCD camera (Hamamatsu C5948) with resolution 640 × 480 pixels in

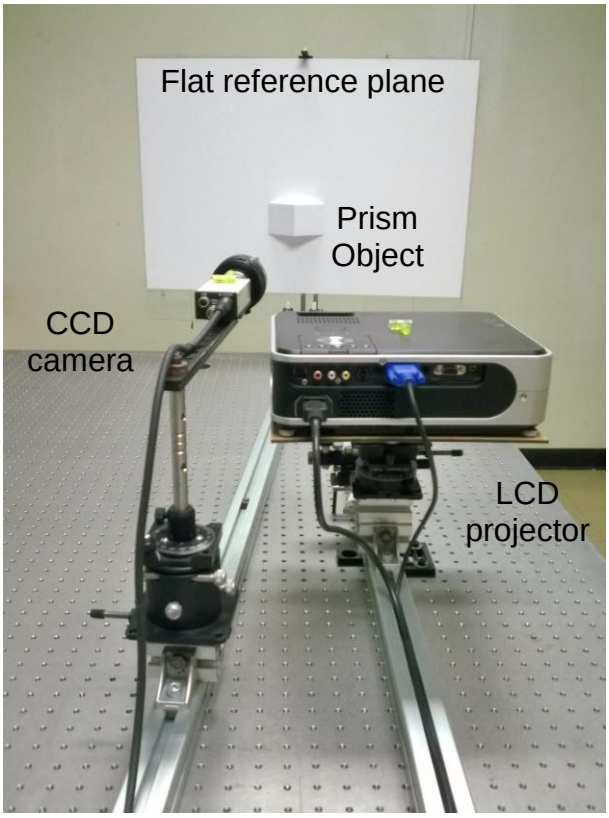

Figure 3.1 An experimental setup for implementing the FTP-based profilometry.

8.3 mm × 6.3 mm sensor area. Lens (AF Nikkor, f=50mm, *f*/1.4D) was used to produce images on the CCD sensor. The axes of the projector and the camera formed the angle θ of 28°.

The isosceles triangle prism shown in Fig. 3.2 with dimension of 13 cm ×7 cm × 4 cm was employed as the test object and installed in the flat reference plane. The sinusoidal grating patterns were projected from the LCD projector. The grating patterns deformed by the object and the reference plane were recorded by using the CCD camera and saved into tiff format. The distances l_0 and d were 100 cm and 53 cm, respectively. The grating pitch projected at the angle θ = 0°on the reference plane was 5.35 mm. According the FTP technique, the reconstructions are done after

the phase modulation can be extracted from each row of the grating image deformed by the object. All computations were done by using Matlab.

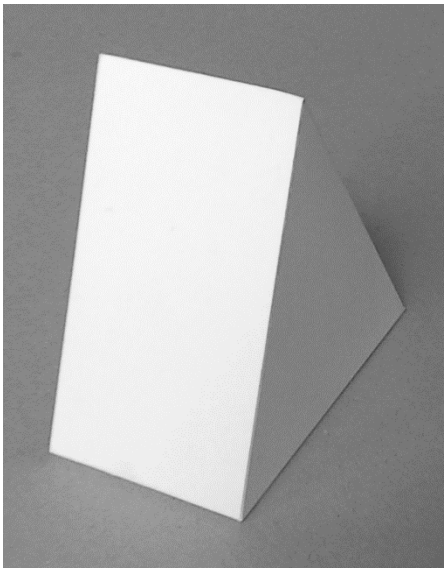

Figure 3.2 An isosceles triangular prism object.

Chapter 4

Results and Discussions

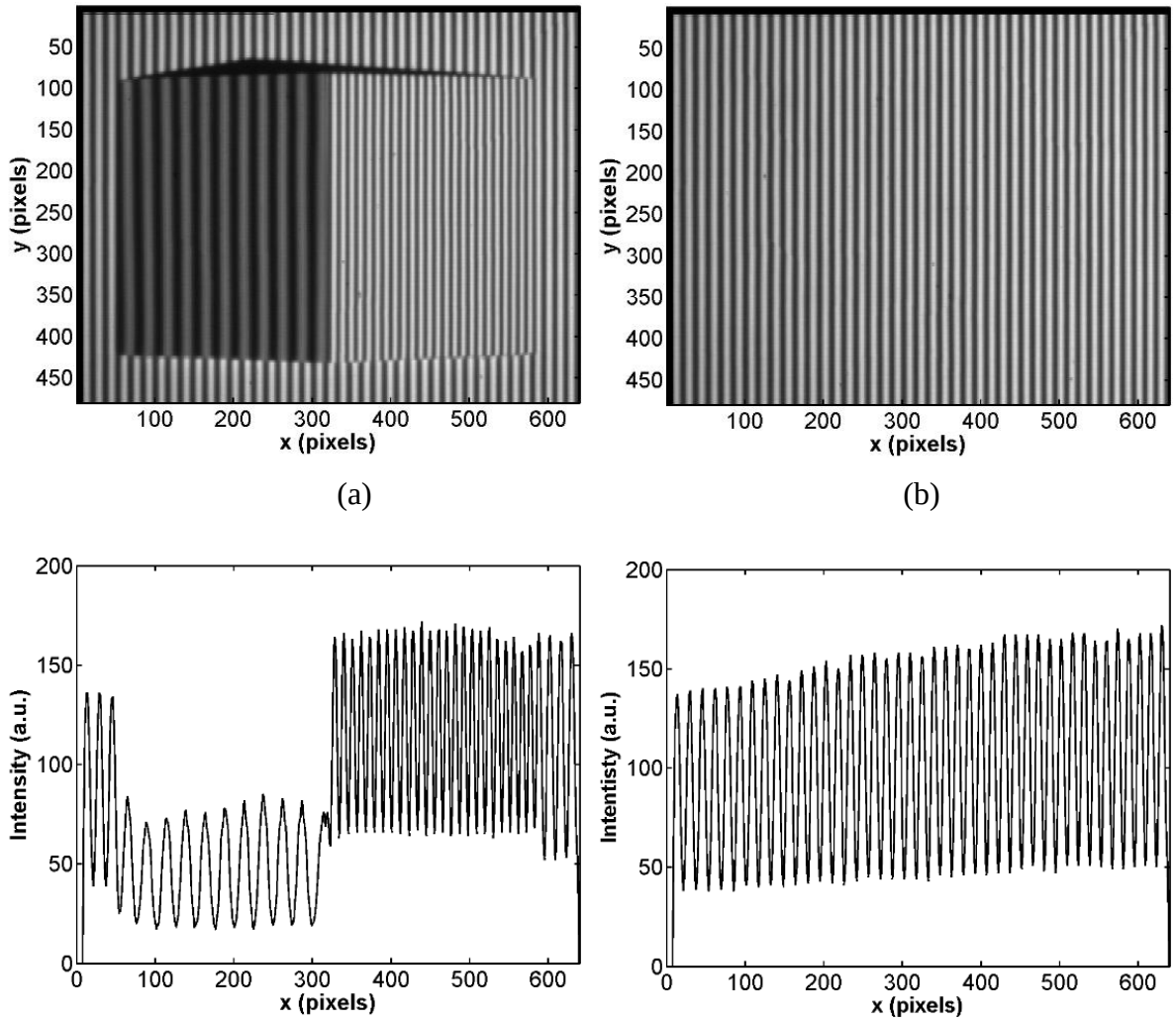

Fig. 4.1Grating images deformed by (a) the isosceles triangle prism object and (b) the reference plane. Intensities scanned at the row 100th of the grating images shown in (c) Fig. a and (d) Fig. d, respectively.

Figures 4.1 (a) and (b) show the grating images deformed by the prism object and the reference plane, respectively. In Fig. 4.1(a), the projection angle causes an elongation of the grating pattern incident on the left side of the prism and a pattern compression on the right side. Consequently, an irradiance and a pitch of the deformed gratings on the left side become lower and broader than those on the other side, respectively. Black areas appeared immediately on top of the pattern deformed by the object correspond to the shadows of the prism. The irradiance of

the grating deformed by the screen varies slightly since the reference plane has a zero height. The intensities scanned at the row 100th of the corresponding deformed grating images are shown in Figs. 4.1 (c) and (d). Due to different reflectivity and height, the two images have different dc bias levels and intensity variations. It is worth mentioning that Fig. 4.1(c) exhibits signal discontinuity around the middle of the signal scanned from the grating deformed by the prism object. This middle signal correspond to the prism peak. The discontinuity occurs because the grating pattern is compressed by the height around the peak position. When the grating pitch incident on the peak is narrow, the compressed grating pattern cannot be resolved by the imaging system of the camera. This may cause wrong phase modulation encoded into the deformed grating.

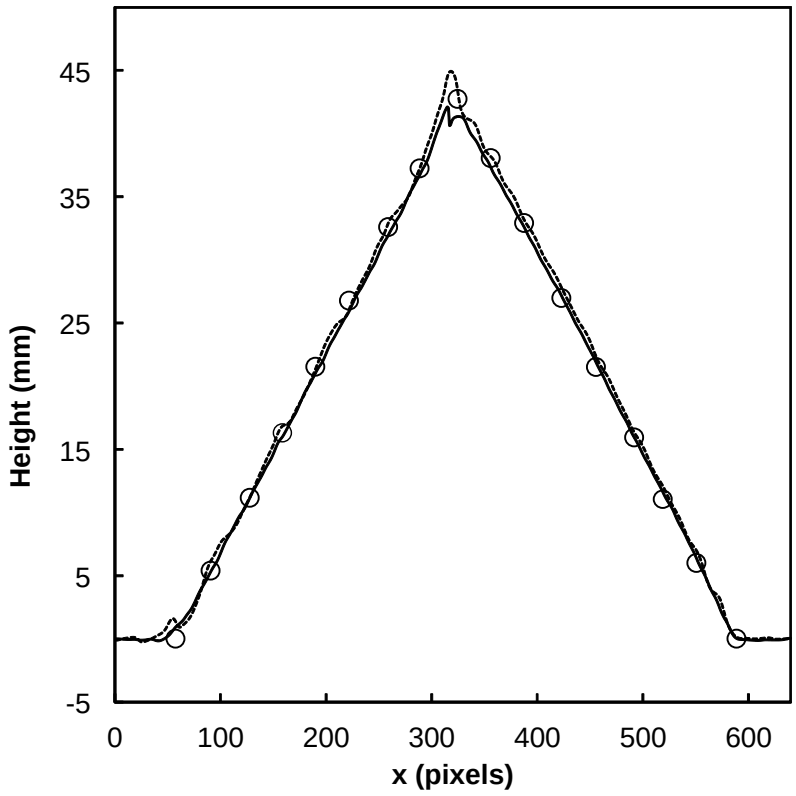

Fig. 4.2 Height reconstructions of the prism generated by using the conventional FTP and the first-order derivative of the Gaussian function.

Figure 4.2 shows the height distributions of the prism object obtained by using the conventional FTP and the proposed first-order derivative of the Gaussian function dilated by the dilation factor *a* of 0.5. The solid line represents the height reconstructed by using the Gaussian wavelet, while the dot line is the result obtained by the conventional FTP. The circle sign corresponds to the height measured through direct physical contact of the prism object with a digital height gauge (Moore and Wright, MW190-30DBL) having an accuracy of 0.01 mm. It can

be observed that the conventional FTP fails to reconstruct the 3D prism profile. It is obvious that its reconstructed surface is indeed not smooth. The base does not have zero height and the peak of the prism does not have correct height. This may be caused by the inherent ringing artifacts of the rectangular band-pass filter together with the degradation of the desired fundamental frequency of the grating pattern by the zero-order spectrum. In contrast, although the prism peak cannot be correctly reconstructed, the use of the first-order derivative of the Gaussian function gives smoother surface profile and better height. This is mainly because the amplitude variation of the Gaussian wavelet in the space and the spatial frequency domains are smooth, removing the ringing artifacts.

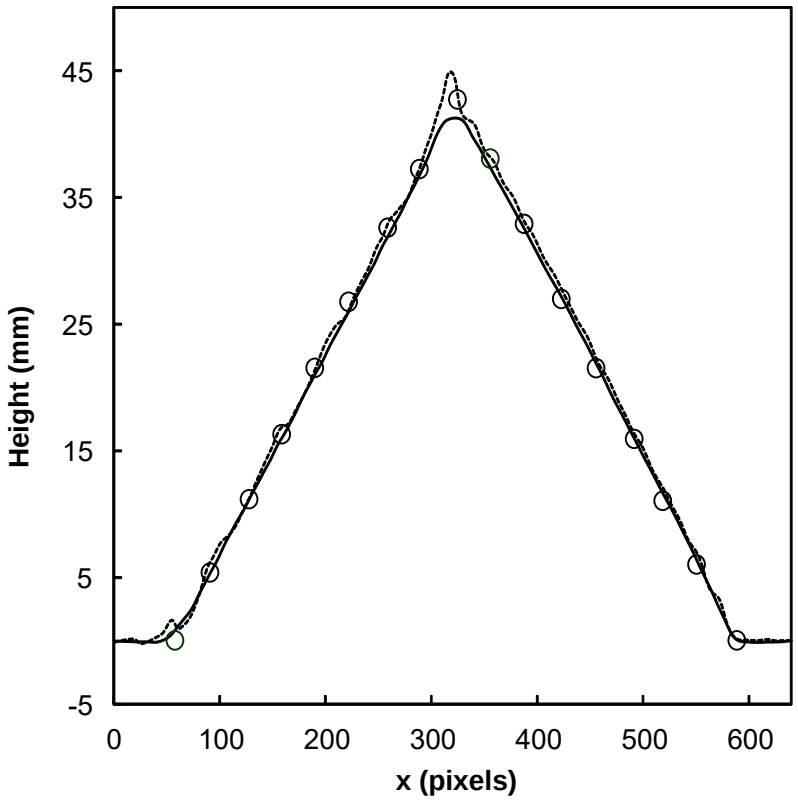

Fig. 4.3 Height reconstructions of the prism generated by using the conventional FTP and the second-order derivative of the Gaussian function.

The comparison of the reconstructed heights obtained by using the conventional FTP and the Mexican hat wavelet dilated by the same dilation factor is shown in Fig. 4.3. It is apparent that in comparison with the results shown in Fig. 4.2, the second-order derivative of the Gaussian function does not only reconstruct smoothly and accurately the prism surface, but also producing symmetrical peak shape. However, since the discontinuous grating signal at the peak gives wrong

phase modulation, a sharp shape of the peak cannot be reconstructed. In comparison with the measurement result done by the digital height gauge, the error in measurement of the peak height is 3.22%. This improvement is achieved because the stop-band of this wavelet around the zero frequency shown in Fig. 2.5(b) is broader than the first-order derivative of the Gaussian function. Therefore, the Mexican hat wavelet can suppress more low frequency components. This results in better localization of the desired fundamental frequency spectrum.

Chapter 5
Conclusions

We have studied the implementation of the FTP-based 3D profilometry by using the first- and the second-order derivatives of the Gaussian function. The advantage of using the Gaussian wavelets over the conventional rectangular filter of the conventional FTP is that they can simultaneously eliminate the zero order spectrum and localize particular frequency components of the desired fundamental spectrum of the deformed grating signals without causing the ringing artifacts on the reconstructed shape.

The experimental results show that in comparison with the first-order derivative of the Gaussian function, the height measurements by using the second-order derivative of the Gaussian function is more accurate. This is because the second-order derivative of the Gaussian function has broader stop-band around the zero frequency. Therefore, this wavelet filter can suppress more efficient the low frequency components.

References

1. M. Takeda, H. Ina and S. Kobayashi, “Fourier-transform method of fringe-pattern analysis for computer-based topography and interferometry,” J. Opt. Soc. Am. 72, 156 - 160 (1982).
2. M. Takeda and K. Mutoh, “Fourier transform profilometry for the automatic measurement of 3-D object shapes,” Appl. Opt. 22(24), 3977 - 3982 (1983).
3. D.R. Burton, A.J. Goodall, J.T. Atkinson and M.J. Lalor, “The use of carrier frequency shifting for the elimination of phase discontinuities in Fourier transform profilometry,” Opt. Lasers Eng. 23, 245 - 257 (1995).
4. H.M Yue, X.Y. Su and Y.Z. Liu, “Fourier transform profilometry based on composite structured light pattern,” Opt. Laser Tech. 39, 1170 - 1175 (2007).
5. E. Hu and F. Haifeng, “Surface profile inspection of a moving object by using dual-frequency Fourier transform profilometry,” Optik 122, 1245 - 1248 (2011).
6. Y. Fu, J. Wu and G. Jiang, “Fourier transform profilometry based on defocusing,” Opt. Laser Tech. 44, 727 - 733 (2012).
7. M. Leonardi, M. Flezar, A. Urbanc and J. Lenarcic, “Application of Fourier transform profilometry in pulmonary function testing,” J. Compt. Inf. Tech. 2, 223 - 231 (1994).
8. M. Leonardi, M. Cucek-Plenicar and J. Lenarcic, “Application of Fourier Transform Profilometry for Measurements of Human Back,” in *Studies in Health Technology and Informatics 37*, Eds. J.A. Sevastik and K.M. Diab, IOS Press, 319 - 322 (1997).
9. F. Lilley, M. J. Lalor and D. R. Burton, “Robust fringe analysis system for human body shape measurement,” Opt. Eng. 39, 187 - 195 (2000).
10. L. Chen and C. Huang, “Miniaturized 3D surface profilometer using digital fringe projection,” Meas. Sci. Tech. 16, 1061 - 1068 (2005).
11. A. Hanafi, T. Gharbi and J. Cornu, “In vivo measurement of lower back deformations with Fourier-transform profiometry,” Appl. Opt. 44, 2266 - 2273 (2005).
12. L.D. Stefano and F. Boland, “Solder-paste inspection by structured light methods based on phase measurement,” Proc. SPIE 2899, *Automated Optical Inspection for Industry*, 702 (1996).
13. C. Quan, C.J. Tay, X.Y. Heb, X Kang and H.M. Shang, “Microscopic surface contouring by fringe projection method,” Opt. Lasers Eng. 34, 547 - 552 (2002).
14. H. Yen, D. Tsai and J. Yang, “Full-field 3-D measurement of solder pastes using LCD-based phase shifting techniques,” IEEE Trans. Elect. Pack. Manu. 29, 50 - 57 (2006).

15. T. Hui and G. K. Pang, “Solder paste inspection using region-based defect detection,” Int. J. Adv. Manu. Tech. 42, 725 - 734 (2009).
16. D. Hong, H. Lee, M. Y. Kim, H. Cho and J. Moon, “Sensor fusion of phase measuring profilometry and stereo vision for three-dimensional inspection of electronic components assembled on printed circuit boards,” Appl. Opt. 48, 4158 - 169 (2009).
17. S. Tan, D. Song and L. Zeng, “Tracking fringe method for measuring the shape and position of a swimming fish,” Opt. Commun. 173, 123 - 128 (2000).
18. P. Cheng, J. Hu, G. Zhang, L. Hou, B. Xu and X. Wu, “Deformation measurements of dragonfly’s wings in free flight by using Windowed Fourier Transform,” Opt. Laser Eng. 46, 157 - 161 (2008).
19. G.H. Wua, L.J Zeng and L.H. Ji, “Measuring the wing kinematics of a moth (Helicoverpa Armigera) by a two-dimensional fringe projection method,” J. Bionic Eng. 5, 138 - 142 (2008).
20. G. S. Spagnolo, D. Ambrosini and D. Paoletti, “Low-cost optoelectronic system for three-dimensional artwork texture measurement,” IEEE Trans. Image Proc. 1, 390 - 396 (2004).
21. G. Sansoni and F. Docchio, “3-D optical measurements in the field of cultural heritage: The case of the Vittoria Alata of Brescia,” IEEE Trans. Inst. Meas. 5, 359 - 368 (2005).
22. P.J. Cobelli, A. Maurel, V. Pagneux and P. Petitjeans, “Global measurement of water waves by Fourier transform profilometry,” Exp. Fluids 46, 1037 - 1047 (2009).
23. A. Martinez, J.A. Raya, R.R. Cordero, D. Balieiroc and F. Labbe, “Leaf cuticle topography retrieved by using fringe projection,” Opt. Lasers Eng. 50, 231 - 235 (2012).
24. B.C. Redman, S.J. Novotny, T. Grow, V. Rudd, N. Woody, M. Hinckley, P. McCumber, N. Rogers, M. Hoening, K. Kubala, S. Shald, R. Uberna, T. D'Alberto, T. Hoft, R. Sibell, and F.W. Wheeler, “Stand-off Biometric Identification using Fourier Transform Profilometry for 2D+3D Face Imaging,” CLEO 2011: Applications and Technology (CLEO: A and T) paper: ATuF4.
25. M.A. Gdeistat, D.R. Burton, M.J. Lalor, “Eliminating the zero spectrum in Fourier transform profilometry using a two-dimensional continuous wavelet transform,” Opt. Commun. 266, 482 - 489 (2006).
26. A Dursun, S Özder, FN Ecevit, “Continuous wavelet transform analysis of projected fringe patterns,” Meas. Sci. Technol. 15, 1768- (2004).
27. S. Mallat and, W.L. Hwang, “Singularity detection and processing with wavelets,” IEEE Trans. Inf. Theory 38, 617 - 643 (1992).

Curriculum Vitae

1. Name: Joewono WIDJAJA

2. Current position: Professor

3. Educational background:

1986 Bachelor of Engineering (Electronic), Satya Wacana Christian Univ., Indonesia

1991 Master of Engineering (Electronic), Hokkaido University, Japan

1994 Doctor of Engineering (Electronic), Hokkaido University, Japan

4. Award and Honor:

1991 Asami Award, Hokkaido University, Japan

2008 Galileo Galilei Award, International Commission for Optics

2009 Distinguished researcher, Suranaree University of Technology

4. Field of specialization: Optical information processing

5. Patent:

Two Japan patents

6. Publications

More than 50 peer-reviewed papers and proceedings